Computational Materials Science 170 (2019) 109149

Contents lists available at ScienceDirect

Computational Materials Science

journal homepage: www.elsevier.com/locate/commatsci

Nanoscale contact behavior of (1 1 1) fcc metallic surfaces

Milad Khajehvand[a,*], Henri Seppänen[b], Panthea Sepehrband[a]

[a] Department of Mechanical Engineering, Santa Clara University, Santa Clara, CA 95053, USA
[b] Kulicke & Soffa Industries, Inc., Santa Ana, CA 92705, USA

ARTICLE INFO

Keywords:
Jump-to-contact
Interfaces
Dislocation multiplication
Cross-slip
Molecular dynamics

ABSTRACT

With the use of molecular dynamics simulations, the contact between two substrates made of the same material is investigated for three different fcc metals: Al, Cu, and Ag. For this purpose, two misoriented substrates containing (1 1 1) planes parallel to their surfaces are placed at varied interfacial separations and allowed to form a contact. While JC happens in all three materials, it is shown that, as opposed to Al and Ag, Cu exhibits a smooth jump-to-contact (JC) behavior, meaning that for separations just above the critical distance for JC, the two surfaces get closer to each other, but they do not form a contact. On the other hand, for separations below the critical distance, JC occurs, and dislocations are generated at the interface due to the misorientation between substrates. It is seen that under favorable conditions, the interfacial dislocations can multiply, primarily because of the strain that exists in the system due to the initial interfacial separation. The possibility of occurrence of dislocation multiplication is found to be higher at high contact temperatures, high strain values, and low misorientation angles. Also, Al is found to be less prone to dislocation multiplication, compared to Ag and Cu. Most importantly, it is observed that the predominant mechanism for dislocation multiplication in Al is cross-slip of interfacial dislocations, whereas in Ag and Cu it is the nucleation of partial dislocations from the interface.

1. Introduction

Understanding the contact behavior of metallic substrates is important to address several problems in technological applications that involve phenomena such as adhesion, friction, wear, and indentation. At nanoscale, it has been shown that when two metallic surfaces are brought toward each other, at some critical distance atoms on the surfaces jump together. The so-called jump-to-contact (JC) phenomenon, first suggested by Gimzewski and Moller [1], has been observed to occur, both experimentally [1–6] and computationally [2,6–11]. JC is the result of a competition between decrease in the energy due to elimination of free surfaces and increase in the energy as a consequence of atomic layers being elastically stretched to fill the interfacial gap [9,11]. Therefore, parameters such as surface energy, elastic modulus, and crystallographic defects generation (because of existence of initial gap and possible misorientation) are expected to affect the JC behavior.

Our previous study [11] has shown that when contact forms between two substrates with misorientations, dislocations form at the interface. Studying the distribution and density of interfacial dislocations is of great importance considering its impact on the diffusional mechanisms and phase transformations that may occur following the contact [12,13]. In addition, interfacial dislocations may interact with other crystallographic defects in the system or even cause generation of new defects in the presence of strain. For instance, it has been shown that small angle (1 1 1) twist grain boundaries and semi-coherent (1 1 1) interfaces, which are similar to the interface after JC when misorientation exists, can act as sinks for point defects [14,15]. It has also been shown that grain boundaries and interfaces can act as nucleation sites for partial dislocations [16–18]. Such behavior is related to the dislocation network at the boundaries [18]. Although several works have studied the dislocation patterns in (1 1 1) twist boundaries [19–21], it is necessary to consider the effect of the initial interfacial gap between substrates when studying the distribution of defects at the interface after JC. The initial interfacial gap effectively causes the system to be under some internal strain after formation of contact. In our recent study [11], dislocation network right after JC in aluminum is investigated and it is shown that although the general pattern of crystallographic defects at the interface after contact is controlled by the misorientation angle (similar to twist boundaries), the size of the initial interfacial gap affects the final density of defects at the interface.

In the present study, using molecular dynamics (MD) simulations, the JC behavior of three fcc metals with various stacking fault energy (i.e., Al, Cu, and Ag) are compared, and the evolution of the resultant dislocations after JC is inspected. The effect of material type,

* Corresponding author.
E-mail address: mkhajehvand@scu.edu (M. Khajehvand).

https://doi.org/10.1016/j.commatsci.2019.109149
Received 14 April 2019; Received in revised form 14 July 2019; Accepted 16 July 2019
Available online 24 July 2019

Table 1
Information about the employed interatomic potentials from [23], including the cutoff distance, lattice constant, melting temperature, intrinsic SFE, unstable SFE, (1 1 1) surface energy, and Young's modulus.

Material	r_c(Å)	$a^{(0\ K)}$ (Å)	T_m (K)	γ_{ISF} (mJ/m^2)	γ_{USF} (mJ/m^2)	$\gamma_{(111)}$ (mJ/m^2)	E (GPa)
Al	6.5	4.032	880	117	158	634	69
Cu	6.5	3.603	1320	53	190	1387	125
Ag	6.0	4.065	1255	26	114	977	78

temperature, strain, and misorientation on the dislocation evolution following contact is investigated and the mechanism by which dislocation multiplication occurs in different materials is identified.

2. Computational methods

MD simulations are performed utilizing the Large-scale Atomic/Molecular Massively Parallel Simulator (LAMMPS) simulation package [22] and embedded atom method (EAM) interatomic potentials for Aluminum, Copper, and Silver [23]. The three metals are chosen because of their low (Ag), medium (Cu), and high (Al) stacking fault energies (SFEs). Table 1 contains information about the employed interatomic potentials. Time integration of equations of motion is carried out with a timestep of 2 fs. Simulations are performed while keeping the temperature and pressure constant (i.e., *NPT* ensemble), using the Nosé-Hoover thermostat and barostat [24–26]. Three temperatures of 300 K, 428 K, and 450 K are chosen for this study since they are homologous temperatures ($T_H = 0.34\ T_m$). Homologous temperatures are used in order to differentiate between the effects of temperature and melting temperature. Axes x, y, and z of the simulation cell are along the $[1\bar{1}0]$, $[11\bar{2}]$, and [111] crystallographic directions of an fcc crystal, respectively. Periodic boundary conditions are used in the x and y-directions.

Initial atomic configurations with different misorientation angles ($0° \leq \theta \leq 21.79°$), corresponding to the coincidence site lattice angles, are created using the same approach explained in [11]. First, two in-registry aluminum substrates are created, each containing 12, (1 1 1) atomic layers parallel to the xy-plane. Next, the upper and lower substrates are rotated about the z-axis of the simulation cell by $\theta/2$, in opposite directions. Then, all atomic configurations are replicated in the x and y-directions, so that approximately 300,000 atoms exist in the simulation cell. The top two layers of the upper substrate and the bottom two layers of the lower one are kept fixed during the simulations. A constant number of Newtonian layers (i.e., 10 layers per each substrate) is used in all simulations. Energy minimization is performed at 0 K using the conjugate gradient method that is implemented in LAMMPS. The system is then thermalized at the desired contact temperature for 20 ps, while keeping pressure constant (i.e., zero) along the periodic directions (i.e., x and y-directions). Finally, the two substrates are displaced to varied interfacial separations and for each separation, the simulation is performed using the *NPT* ensemble for 20 ps (in Section 3.1) or 200 ps (in Section 3.2).

In order to identify the occurrence of a complete JC, similar to [11], a deviation parameter, $D(t)$, is defined as follows and computed throughout the simulations:

$$D(t) = \frac{|h(t) - d|}{d}, \tag{1}$$

where $h(t)$ is the interfacial separation (i.e., the distance between contacting layers) as a function of time, and d is the interplanar spacing of (1 1 1) planes in a perfect crystal, for a given material and temperature. $h(t)$ is calculated by subtracting the average of z-positions of atoms on the lower substrate's surface from the average of z-positions of atoms on upper substrate's surface. When the value of D drops to a positive value close to zero, it indicates that JC has occurred. In this work, the average of D in the last 2 ps of simulations, D_{ave}, is used as a parameter for determining the occurrence of JC.

When JC occurs, the strain in the system, i.e., ε, can be calculated as follows:

$$\varepsilon\ (\%) = \frac{1}{2} \times \frac{(h_{initial} - h_{final})}{(number\ \ of\ \ Newtonian\ \ layers\ \ per\ \ substrate) \times d} \times 100, \tag{2}$$

where $h_{initial}$, the initial interfacial distance (i.e., $h(t = 0\ ps)$), is always set to be a pre-selected multiple (i.e., n) of interplanar spacing:

$$h_{initial} = n \times d, \tag{3}$$

and h_{final}, the final interfacial distance (i.e., $h(t = 20\ ps)$), is almost equal to d, i.e., $h_{final} \approx d$. Also, a constant number of Newtonian layers per substrate (i.e., 10) is chosen for this study. Therefore:

$$\varepsilon\ (\%) \approx 5 \times (n - 1). \tag{4}$$

For instance, the strain in a system with $h_{initial} = 2.3\ \times d$, after occurrence of JC, is almost equal to $\varepsilon = 6.5\%$. It is worth mentioning that h_{final} in Eq. (2) is slightly greater than d since the two contacting layers are also a bit strained due to existence of the initial gap. However, for the purpose of ease of calculations, it is assumed to be negligible. As a result, the true ε in the system is slightly lower than the values reported in this work. Additionally, it is important to note that the strain values would be lower if a higher number of Newtonian layers per substrate had been used (see Eq. (2)).

3. Results and discussion

3.1. Jump-to-Contact (JC) behavior

It is generally accepted that the JC phenomenon is a balance between the attractive forces between atoms on the free surfaces and the stiffness of material [9,27]. Therefore, the JC behavior is expected to depend on the material properties and temperature. The JC behavior of different materials (i.e., Al, Cu, and Ag) at a range of temperature (i.e., 300 K, 428 K, and 450 K) is simulated. A constant misorientation angle (i.e., 0°) is used in the simulations since in [11], it is shown that misorientation does not affect the critical distance for JC. The simulations are performed for initial interfacial separations in the range of $h_{initial} = n \times d$, where $1.5 \leq n \leq 3.5$. Values of d, $n_{critical}$ (i.e., the critical distance for JC in terms of multiple of d), $h_{critical}$ (i.e., the critical distance for JC in Å), and $\varepsilon_{critical}$ (i.e., the maximum strain present in the system upon occurrence of JC) are calculated as listed in Table 2. The results show that for any given material, the critical distance for JC increases by increase in temperature. The occurrence of JC at greater

Table 2
Values of d, $n_{critical}$, $h_{critical}$, and $\varepsilon_{critical}$ calculated from our MD simulations (increase in the value of d at higher temperatures is due to thermal expansion).

Temperature (K)	300			428			450		
Material	Al	Cu	Ag	Al	Cu	Ag	Al	Cu	Ag
d(Å)	2.349	2.092	2.364	2.371	2.098	2.369	2.372	2.099	2.370
$n_{critical}$	2.4	2.5	2.3	2.4	2.5	2.4	2.5	2.6	2.4
$h_{critical}$(Å) = $n_{critical} \times d$(Å)	5.637	5.230	5.437	5.690	5.245	5.685	5.930	5.457	5.688
$\varepsilon_{critical}$ (%)	7.0	7.5	6.5	7.0	7.5	7.0	7.5	8.0	7.0

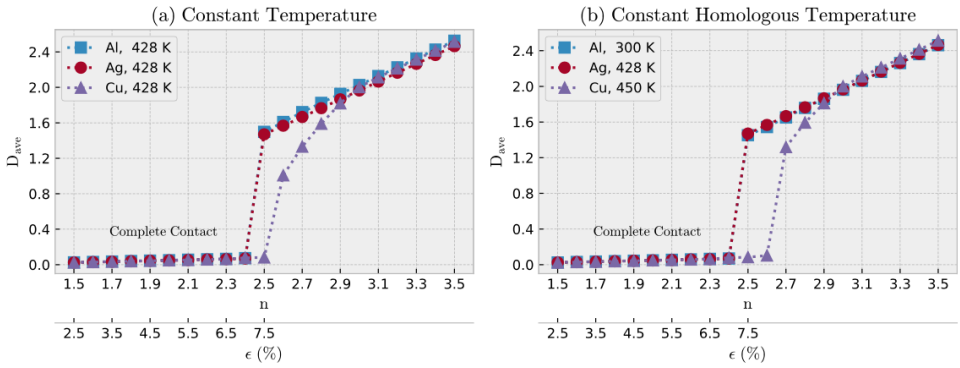

Fig. 1. "D_{ave} vs. n" and "D_{ave} vs. strain" curves showing a comparison of the JC behavior of the three metals at a (a) constant temperature and (b) constant homologous temperature.

separations at higher temperatures is due to the larger magnitude of atomic vibrations, which increases the possibility of the surface atoms coming into a close vicinity of the atoms on the opposing surface.

The JC behavior of the three metals at a constant temperature (i.e., 428 K) is presented in Fig. 1(a). In this figure, the y-axis corresponds to D_{ave} (i.e., the average of D in the last 2 ps of simulations) and the x-axis is $n = h_{initial}/d$ (i.e., a normalized form of the initial interfacial distance). The secondary x-axis corresponds to the values of strain present in the system for the cases in which JC occurs. Although the normalized critical distance for JC to occur is almost the same for all the three materials (i.e., $n = 2.4$ for Al and Ag and $n = 2.5$ for Cu), it is seen that Cu follows a different trend just above the critical distance. This shape of curve for Cu implies that, below a certain level of separation but above a critical distance, the two Cu substrates get stretched, the free surfaces get closer to each other, but they do not form a complete contact. A similar behavior was observed for the other two temperatures (i.e., 300 K and 450 K). In Fig. 1(b), the JC behavior of the metals is compared for a constant homologous temperature. The same behavior is observed, which indicates that the difference in behavior of Cu compared to Al and Ag may not be related to atomic vibrations that have arisen from the difference in the melting temperatures. This observation (i.e., the difference in the shape of the curve of Cu compared to the other two metals, for distances right above $n_{critical}$), may be related to the higher (111) surface energy and Young's modulus (see Table 1) of Cu. For separations just above the $n_{critical}$, it is favorable for the Cu system that the two free surfaces form a contact and decrease the total energy of the system by removal of free surfaces, but the high Young's modulus prevents it. In this case, the gradient of the force that is being applied on the surface atoms by the atoms on the opposing surface never exceeds the "effective spring constant" by which the surface atoms are held [27]. The effect of elastic properties of metals on their JC behavior is reported by Untiedt et al [2], where through a combination of scanning tunneling microscopy and mechanically controllable break junctions experiments, it was shown that while JC always occurs for atomic size tips such as Au and Ag, it does not occur for the ones with superior elastic properties like W. It seems that our observation in this work is in agreement with theirs, in terms of the fact that the elastic properties of materials play an important role in their JC behavior. However, the effect of surface energy, as the driving force for JC, should not be neglected, especially in the case of JC between two surfaces (as opposed to atomic size tips which is studied in [2]).

The parameter D_{ave} that is used to determine the occurrence of contact accurately predicts the occurrence of a "complete contact" between surfaces across the interface (cases with $n \leq n_{critical}$ in Fig. 1(a)). An example of such case is shown in Fig. 2(a) and (b), where two surfaces have come to a proximity of approximately one interplanar spacing from one another in the final state. However, it should be noted that for the cases with n right above the $n_{critical}$, it is possible for the system to present a local contact, as shown in Fig. 2(c) and (d), for two different cases. These local contacts can be important in some applications due to the ability of the system to pass electrical current, as discussed in [27]. However, as represented by the triangles in the 2D map of interfacial distance in Fig. 2(c), such local contacts lead to formation of a hard to predict dislocation network. The generated dislocation network is the results of non-uniform strain in the system that is arisen from local contacts. Basically, as a result of local contact, an unpredictable dislocation network (that is originated form random atomic movement) gets generated which inhibits a systematic analysis of the dislocation evolution after contact formation, which is of the main interest of this work (as will be discussed in Section 3.2). Therefore, to avoid additional complexity, we focus on the cases that form complete contacts. Yet, local contact remains an important and interesting phenomenon that should be studied separately.

3.2. Distribution and density of dislocations after contact

3.2.1. Interfacial dislocations after JC

As discussed in [11], For misorientation angles in the range of $0° < \theta \leq 21.79°$ (and similarly $38.21° \leq \theta < 60°$), after occurrence of JC, dislocations are generated at the interface to accommodate the misorientation between the two substrates. In this work, it is seen that the general pattern of interfacial dislocations after occurrence of JC is similar in the three metals. As an example, Fig. 3 shows the results of contact simulation for two Cu substrates at 450 K, which were initially misoriented by 4.40° and placed at $1.9 \times d$ from each other. The two Cu substrates, after occurrence of JC, are shown in Fig. 3(a). Fig. 3(b) shows the dislocations that exist between the two contacting layers (i.e., colored as red and yellow in Fig. 3(a)). Shockley partial dislocations with Burgers vectors of $1/6\langle 112\rangle$ and perfect dislocations with Burgers vectors of $1/2\langle 110\rangle$ are colored as green and blue, respectively. The triangular network of Shockley partial dislocations can be better seen in Fig. 3(c), where a top-view image of the network of interfacial dislocations is presented. Moreover, Fig. 3(d) shows that the Shockley partial dislocations separate the regions of atoms with perfect fcc local crystal structure (colored as purple) from the stacking fault regions (i.e., atoms with HCP local crystal structure, colored as red). The white atoms in Fig. 3(d) are the atoms that do not possess any known local crystal structure. The effect of misorientation on the distribution and density of dislocations has been discussed in [11] in detail. In brief, for the range of misorientation angles studied (i.e., $0° < \theta \leq 21.79°$), as

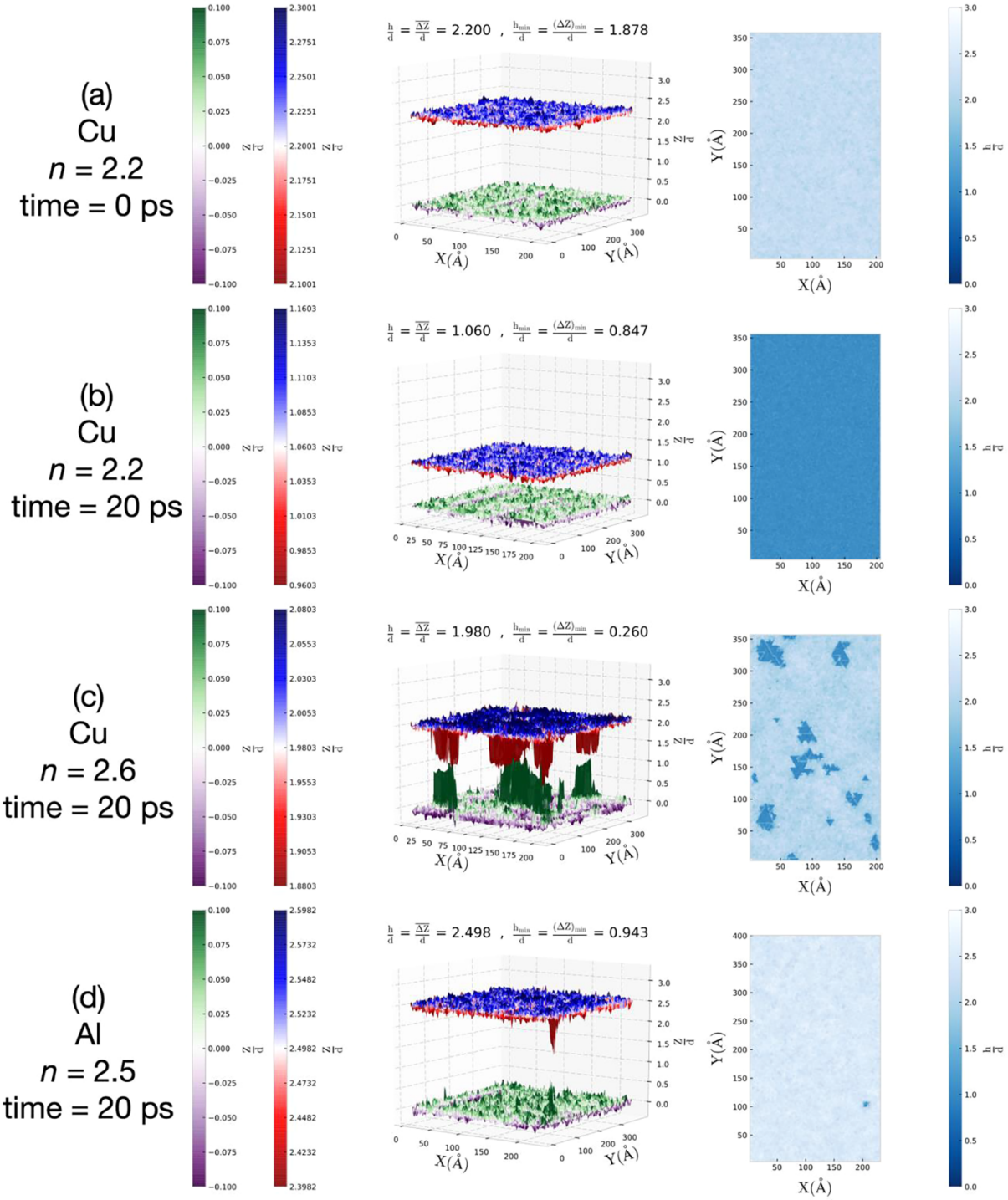

Fig. 2. 3D representations of contacting layers and 2D maps of interfacial distance for three cases presented in Fig. 1(a). (a), and (b)–(d) correspond to the initial and final states of simulations, respectively.

misorientation angle deviates from 0°, the triangles become smaller and the dislocation junctions get closer to each other.

3.2.2. *Multiplication of interfacial dislocations*

Depending on the material type, contact temperature, strain, and misorientation angle, simulation results have shown that following contact, the density of resultant interfacial dislocations may increase, through dislocation multiplication. Occurrence of dislocation multiplication is important since it significantly affects both the distribution and the density of dislocations. Dislocation evolution after JC is studied

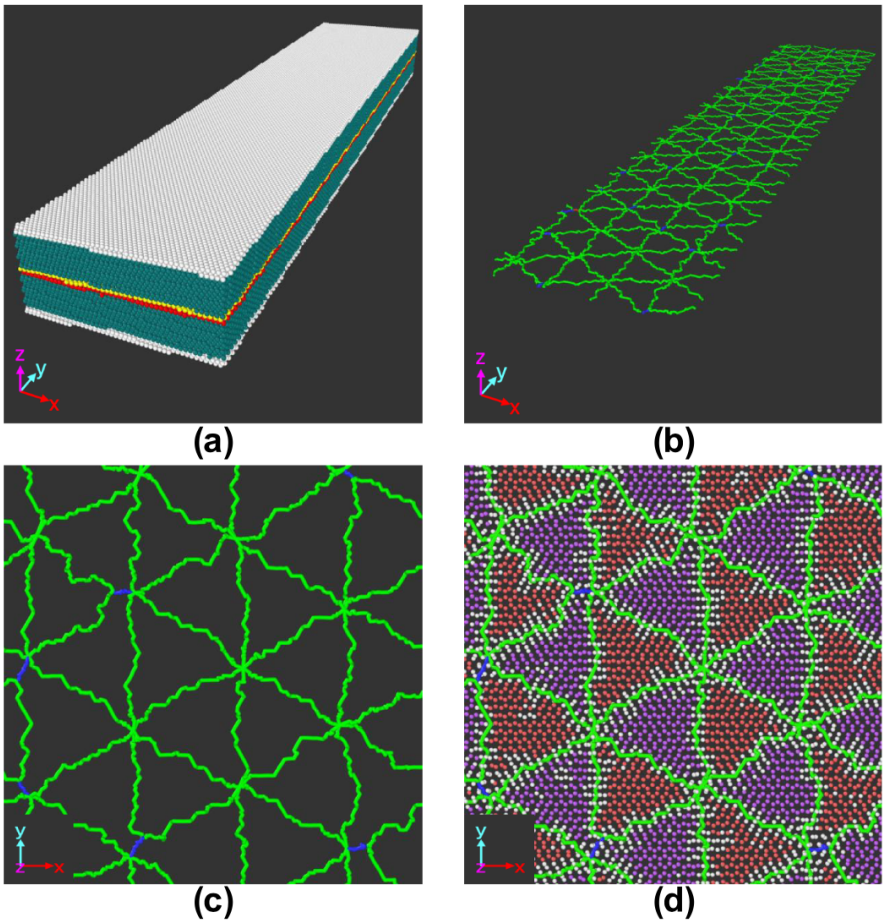

Fig. 3. Snapshots of the simulation of Cu, misorientation: 4.40°, temperature: 450 K, strain: 4.5% case, after occurrence of JC. (a) Shows a perspective view of the system in which the two contacting layers are colored by yellow and red. (b) Shows a perspective view of the dislocation network that exists between the two contacting layers shown in (a). Shockley partials and perfect dislocations are colored as green and blue, respectively. (c) and (d) show top view images of a 110 Å × 110 Å portion of the interface. fcc, HCP, and disordered atoms are colored as purple, red, and white, respectively. Detection of dislocations is done using the dislocation analysis modifier [28] of OVITO [29].

for: the three materials, the three temperatures, and three strain values (i.e., 4.5%, 5.5%, and 6.5%), at a constant misorientation angle (i.e., 2.45°). Fig. 4 shows the evolution of total dislocation density as a function of simulation time, for all of the 27 combinations. For all cases, dislocation density increases (from 0 m^{-2} to around 10×10^{16} m^{-2}) right after jump to contact. This initial increase is due to the formation of interface dislocations that are discussed in Section 3.2.1. In some of the curves (e.g., curve for Al, temperature: 428 K, and strain: 6.5%), in addition, a secondary increase is observed, which is due to the occurrence of dislocation multiplication. In this section, first the mechanism by which dislocation multiplication occurs (Section 3.2.2.1) is discussed, and then, the effect of material type, temperature, strain, and misorientation angle on the possibility of occurrence of dislocation multiplication is analyzed (Section 3.2.2.2).

3.2.2.1. The mechanism of dislocation multiplication. In order to compare the mechanism by which dislocation multiplication occurs in the three metals, three simulation cases, which lead to dislocation multiplication, are chosen. Those three simulations correspond to Al, Cu, and Ag, in all of which the misorientation is 2.45°, the temperature is 450 K, and the strain is 6.5%. Fig. 5(a) shows the evolution of total dislocation density as a function of simulation time, for these conditions. It is seen that dislocation multiplication occurs faster in Cu and Ag and follows a different trend compared to Al. The notable difference between Al and the other two materials, suggests activation of a different dislocation multiplication mechanism.

The change in the total energy of system (per atom), i.e., ΔE_{total}, as a function of simulation time is shown in Fig. 5(b). For all cases, it is seen that during simulation, the total energy of the system is reduced till a plateau—which represents a steady state—is reached. The initial steep drop in the total energy is due to the occurrence of JC and is the balance of energy changes due to the elimination of free surfaces and formation of interfacial dislocations. At this very beginning stage of simulation, the curve of Al is similar to the curve of Ag and Cu. This behavior agrees with the earlier observation, reported in Section 3.2.1, that for a constant misorientation, the same dislocation network forms in all three materials right after contact. But, later on, when dislocation multiplication happens, the curve of Al clearly takes a different path, compared to the ones for Ag and Cu.

During the simulation, it is observed that as dislocation

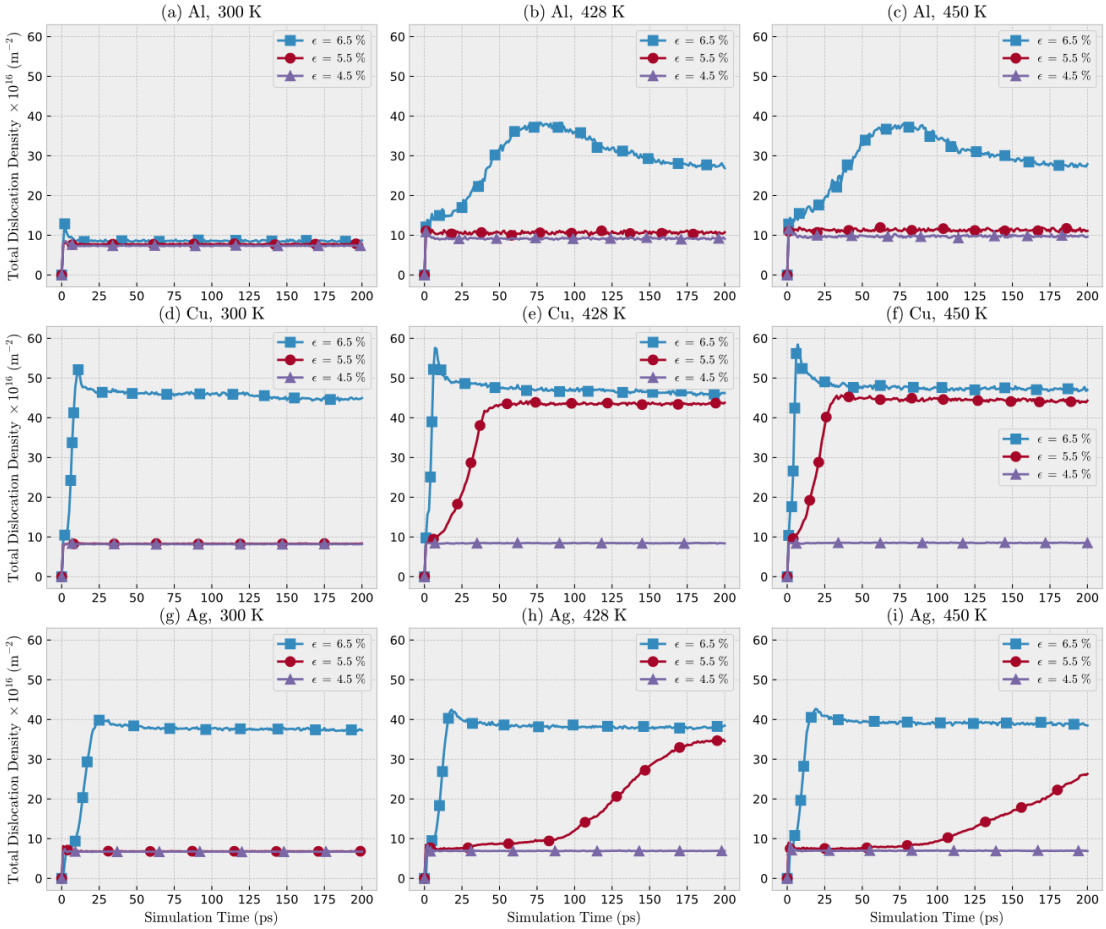

Fig. 4. "Total dislocation density vs. simulation time" plots showing the effect of material type, temperature, and strain on the possibility of occurrence of dislocation multiplication, for a constant misorientation angle (i.e., 2.45°).

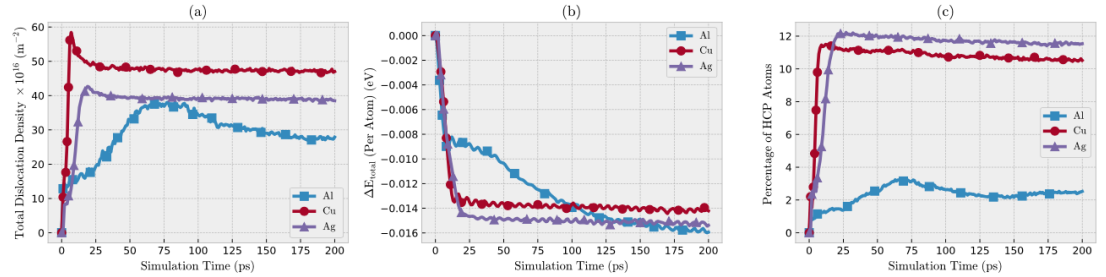

Fig. 5. Evolution of (a) total dislocation density, (b) change in the total energy, and (c) percentage of atoms with HCP local crystal structure throughout the simulation, for Al, Cu, and Ag. For all three simulations, misorientation is 2.45°, temperature is 450 K, and strain is 6.5%.

multiplication occurs, the percentage of atoms with HCP local crystal structure changes. Therefore, to get further insight on dislocation evolution, percentage of HCP atoms during the three simulations is presented in Fig. 5(c). Interestingly, it is observed that the increase in the percentage of atoms with HCP local crystal structure in Al is not as significant as what it is in Ag and Cu. On the whole, all plots in Fig. 5 confirm that there is a difference in the behavior of Al compared to Ag and Cu, in terms of the way dislocation multiplication occurs.

To better inspect the mechanism by which dislocation multiplication occurs, snapshots of the three simulations are provided in Fig. 6. In this figure, the larger images show perspective views of all dislocations present in the system, and smaller images show the side views. Shockley partials are colored as green, perfect dislocations as blue, and stair-rod dislocations as pink. Columns A, B, and C in the figure show dislocation evolution in Cu, Ag, and Al, respectively.

Fig. 6(A1) shows the network of interfacial dislocations in Cu right after JC. In Fig. 6(A2), it is seen that after 3 ps, partial dislocation loops are nucleated, and started propagating on a secondary {1 1 1} slip plane. In the case of Ag, although JC occurs at a later time compared to Cu (see Fig. 6(B1) and (B2)), a very similar behavior is observed (see

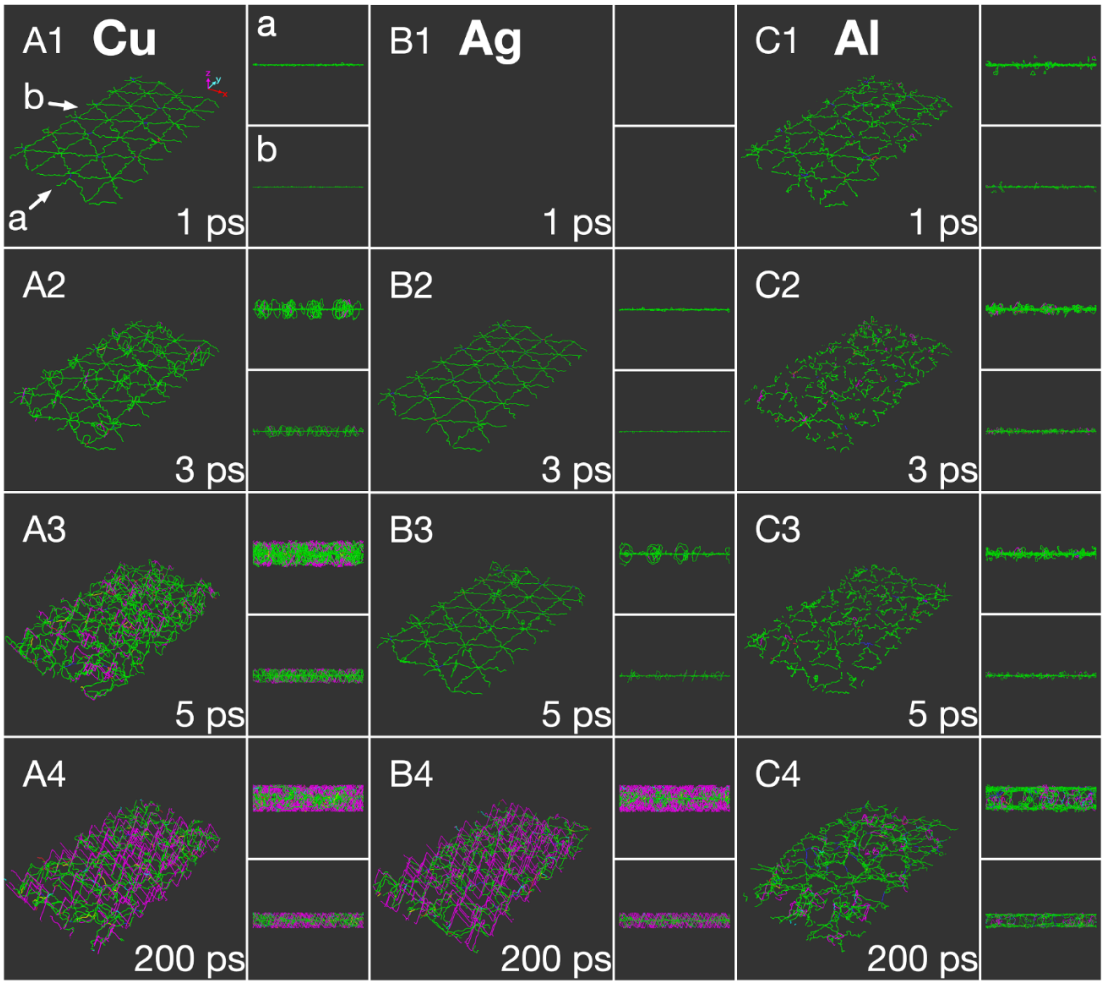

Fig. 6. Snapshots of the systems showing the occurrence of dislocation multiplication throughout the simulations of Cu (A1–A4), Ag (B1–B4), and Al (C1–C4). For all three simulations, misorientation is 2.45°, temperature is 450 K, and strain is 6.5%. In this figure, larger images show perspective views of all dislocations present in the system, and smaller images (labeled a and b) show the side views. Shockley dislocations and stair-rod dislocations are colored as green and pink, respectively. Detection of dislocations is done using the dislocation analysis modifier [28] of OVITO [29]. (To see more snapshots of the simulations, please see Figure f1 of the online supplementary material.)

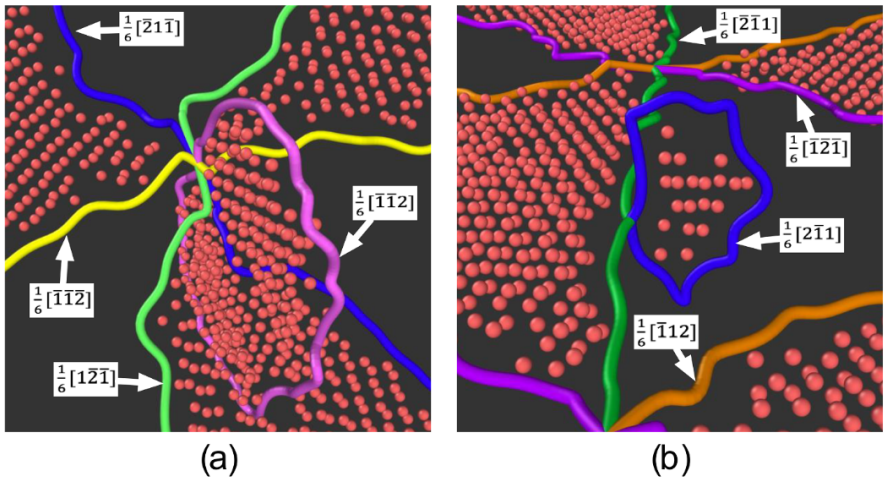

Fig. 7. Nucleation of partial dislocation loops from the network of three crossing sets of dislocations at the interface in Ag (for the same simulation presented in column B of Fig. 6). (a) Shows nucleation from the dislocation junctions (time: 7 ps) and (b) shows nucleation from somewhere along the dislocation segments connecting two junctions (time: 3 ps). All dislocations are Shockley partial dislocations and their Burgers vectors are indicated on the images. The same mechanisms for dislocation nucleation is observed for Cu. Detection of dislocations is done using the dislocation analysis modifier [28] of OVITO [29].

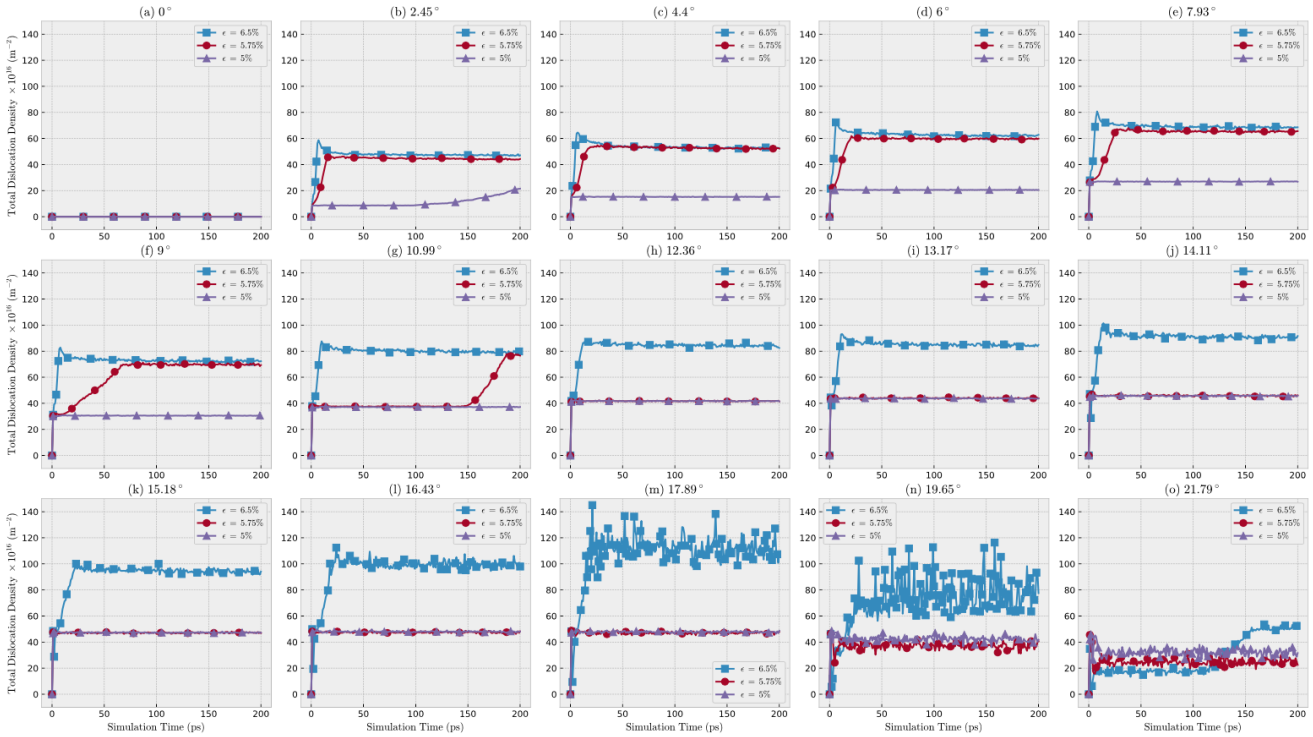

Fig. 8. "Total dislocation density vs. simulation time" plots showing the effect of misorientation on the possibility of occurrence of dislocation multiplication, for a constant material type (Cu) and temperature (450 K).

Fig. 6(B3)). In both materials, the dislocations loops are found to most frequently nucleate at the junction of pre-existing interfacial dislocations, and frequently somewhere close to the middle of the dislocation segment connecting two dislocation junctions. An example of the former and the latter cases in Ag are shown in Fig. 7(a) and (b), respectively. In Fig. 7, Shockley partials are colored based on their Burgers vectors and all atoms with HCP local crystal structure are shown by red dots.

The dislocation loops shown in Fig. 6(A2) and (B3) propagate on the secondary {1 1 1} slip planes until they reach the fixed layers (i.e., atomic layers shown as white in Fig. 3(a)) or another dislocation loop. As this process of dislocation multiplication continues, the sessile stair-rod dislocations (i.e., Lomer-Cottrell dislocations) with Burgers vectors of $1/6\langle 110\rangle$, are generated. These stair-rod dislocations are generated as a result of interaction between partial dislocation loops and are located at the intersection of the {1 1 1} planes (see Fig. 6(A4) and (B4)). It should be emphasized that due to the existence of fixed atomic layers in our simulations, surface absorption of dislocations, which is a way for dislocation annihilation, is impossible to occur. Therefore, as dislocations move on the secondary slip planes and reach the fixed layers, they tend to accumulate. This means that the final steady state of the simulations represents a state of work hardening and the final values of dislocation density in Fig. 4 are affected by this artifact. However, neither the study of mechanism of dislocation multiplication in different metals (Section 3.2.2.1) nor the effect of different simulation parameters on the tendency for dislocation multiplication (Section 3.2.2.2) are affected by this artifact, as they both correspond to the initiation of dislocation multiplication.

As opposed to Cu and Ag, in Al, the nucleation and propagation of partial dislocation loops is not observed. Instead, the pre-existing interfacial dislocations cross-slip to the secondary slip plane. This fact is evidenced by a combination of the following observations:

1. A segregated and disconnected pattern of interfacial dislocations, especially around the junctions (see Fig. 6(C2) and (C3)), is observed. This pattern is a consequence of the recombination of Shockley partial dislocations and the dissociation of the resulted perfect dislocations on the secondary {1 1 1} planes, according to the well-accepted Friedel-Escaig cross-slip mechanism [30–32].
2. At the final stage of the simulation of Al, the majority of dislocations are located near the fixed surfaces, and the areas near the interface is almost free of dislocations (compare Fig. 6(C4) with (A4) and (B4)). Considering the fact that nucleation of partial dislocation loops is not observed in Al, the only way that those dislocations can move to the areas near the fixed surfaces is by occurrence of cross-slip.
3. The increase in the percentage of atoms with HCP local crystal structure is less significant compared to that in Ag and Cu (see Fig. 5(c)). During cross-slip, the stacking fault region gets transferred to the secondary slip plane without a significant generation of new stacking fault. On the other hand, generation of new partial dislocations leads to generation of new stacking fault and a substantial increase in density of atoms with HCP local crystal structure.

On the whole, our observations show that the predominant mechanism for dislocation multiplication in Al is cross-slip of interfacial dislocations, while in Cu and Ag it is the nucleation of Shockley partial dislocation loops from the interface. The fact that cross-slip occurs predominantly in Al is reasonable since Al has the highest intrinsic SFE (i.e., γ_{ISF}) among the three metals (see Table 1). The high value of γ_{ISF} affects dislocation multiplication in Al in two ways: 1) it leads to a small stacking fault width, which in turn increases the possibility of recombination of Shockley partial dislocations and formation of

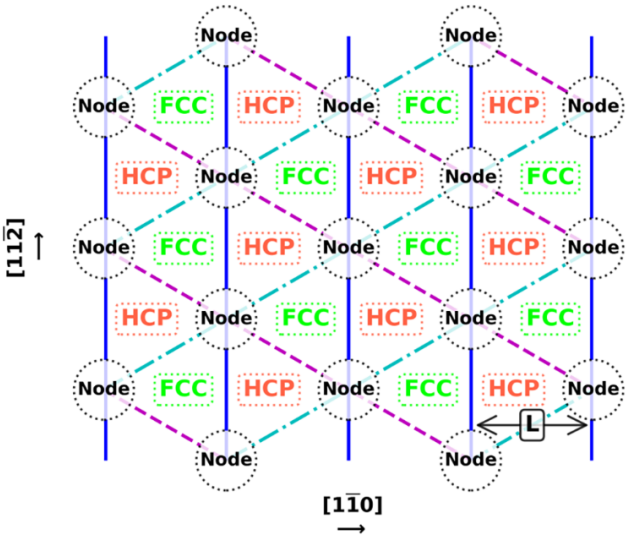

Fig. 9. Schematic diagram showing the network of three crossing sets of Shockley partial dislocations with Burgers vectors of $\frac{1}{6}[11\bar{2}]$ (i.e., solid lines), $\frac{1}{6}[\bar{1}2\bar{1}]$ (i.e., dashed lines), and $\frac{1}{6}[\bar{2}11]$ (i.e., dash dotted lines). The distance between two adjacent parallel dislocations in each set is $L = 3b_P/(4\ \sin(\theta/2))$, where b_p is the magnitude of the Burgers vector of Shockley partial dislocations and θ is the misorientation angle.

constriction that may lead to cross-slip according to the well-known Friedel-Escaig mechanism [30–32]; 2) it suppresses the nucleation of partial dislocations as their nucleation always accompanies formation of stacking fault [33], which is energetically expensive.

For getting a better sense of the difference in the dislocation multiplication behavior of Al, compared to Ag and Cu, the reader is strongly encouraged to watch the online supplementary movies associated with this article. The movies show all types of dislocations and all atoms with HCP local crystal structure in the system. Supplementary Movies S1, S2, and S3 correspond to the total duration of simulations of Cu, Ag, and Al, respectively. Supplementary Movies S4, S5, and S6 show only the initial 20 ps of simulations of Cu, Ag, and Al, respectively.

3.2.2.2. Tendency of dislocation multiplication. The possibility of occurrence of dislocation multiplication as a function of material type was previously shown in Fig. 4. From this figure, it can be understood that the proneness to dislocation multiplication is generally lower in Al, compared to Cu and Ag. This observation is due to Al having a different mechanism for dislocation multiplication, as a result of its significantly high γ_{ISF}. The results presented in Fig. 4 also show that while Cu and Ag are similar in terms of occurrence of dislocation multiplication, the dislocation multiplication happens at a faster rate in Cu, compared to Ag. Considering that the mechanism for dislocation multiplication is the same in these two metals, this observation is interesting because: (1) the energy barrier that a partial dislocation has to overcome in order to nucleate is equal to unstable stacking fault energy (i.e., γ_{USF}), and (2) the expansion of the nucleated dislocation loop enlarges the stacking fault region with energy of γ_{ISF} [34–36]. On the other hand, the expansion of dislocation loop occurs through the two mechanism of dislocation glide and climb that are controlled by Peierls stress and diffusion, respectively [37]. While the higher values of γ_{ISF} and γ_{USF} in Cu compared to Ag (see Table 1), favor dislocation multiplication in Ag, the lower energy barrier for self-diffusion [23] and lower Peierls stress [38] in Cu favor expansion of the dislocation loop in Cu. The results shown in Fig. 4 suggest that for the conditions investigated, dislocation multiplication occurs faster in Cu. However, this observation cannot be easily extended for all cases, and more investigation is required for detailed analysis of dislocation nucleation, and the rate of dislocation multiplication in the cases that cross slip does not happen.

In Fig. 4, it is also seen that for all materials, as temperature increases, it is more likely for dislocation multiplication to occur. Increase in temperature lowers the critical resolved shear stress needed for a dislocation to glide on the secondary slip plane. Also, it is widely accepted that increase in temperature results in higher possibility of cross-slip, as formation of a constriction can be thermally assisted [39,40]. Additionally, Fig. 4 shows that the possibility of dislocation multiplication is higher at higher strain values, which is due to the increase in the value of resolved shear stress on the secondary slip plane.

In order to investigate the effect of misorientation on the occurrence of dislocation multiplication, simulations are performed for all misorientation angles in the range of 0° and 21.79°. These two thresholds are chosen based on the results of our previous study [11], where it was shown that no dislocations exist at the interface for misorientation angles between 21.79° and 38.21°; the dislocation patterns in the range of 38.21° and 60° are found to be similar to the range of 0° and 21.79°. Other parameters are chosen to be in favor of dislocation multiplication to occur (i.e., Cu, temperature of 450 K, and high ε_{el} values of 6.5%, 5.75%, and 5%). The results are presented in Fig. 8. As seen in Fig. 8(a), the density of dislocations is zero for $\theta = 0°$, since there is no mismatch between the two substrates. Fig. 8(b)–(o) show that for $\varepsilon_{el} = 5\%$, dislocation multiplication occurs only for $\theta = 2.45°$; for $\varepsilon_{el} = 5.75\%$, dislocation multiplication occurs only for misorientation angles of $2.45° \leq \theta \leq 10.99°$; and for $\varepsilon_{el} = 6.5\%$, it occurs for all misorientation angles in the range of $2.45° \leq \theta \leq 21.79°$. The results clearly show that the possibility of occurrence of dislocation multiplication is higher at lower misorientation angles.

The rationale behind this general trend can be identified by investigating the effect of misorientation on the distribution of partial dislocations at the interface. In order to consider only the pure effect of misorientation, the structure of {1 1 1} twist boundaries is first investigated, and later on, the effect of initial gap (and the resulted strain) will be taken into consideration. The network of Shockley partial dislocations in a (1 1 1) twist boundary is illustrated schematically in Fig. 9. In this simplified model, the dislocations are assumed to be completely straight and the temperature is considered to be 0 K. De Hosson and Vitek [20] used Hirth and Lothe's description of Frank's formula [33] and showed that the distance between parallel dislocations in each of these three crossing sets is equal to $L = 3b_P/(4\ \sin(\theta/2))$, where b_p is the magnitude of the Burgers vector of Shockley partial dislocations, and θ is the misorientation angle. Based on this formula, as the misorientation angle increases, the distance between partial dislocations decreases, hence, a higher fraction of dislocation junctions (i.e., indicated as nodes in Fig. 9) exists at the interface. Additionally, in [11], using the 2D maps of interatomic distances, we showed that the areas near the dislocation junctions are the areas that have the highest local interfacial distance after contact. Altogether, by increase in the misorientation angle, the overall final interfacial distance (i.e., h_{final}) increases. And, according to Eq. (2), the ε_{el} decreases by the increase in h_{final}, which discourages dislocation multiplication. In sum, the possibility of dislocation multiplication is higher at lower misorientation angles, primarily because of the higher localized ε_{el} value at the dislocation junctions. Since the effect of misorientation on the pattern of dislocations is independent of the material type, and due to the fact that dislocation nodes are the dominant sites for initiation of cross-slip or nucleation of Shockley partials, the same kind of trend is expected for Al and Ag.

4. Conclusions

In summary, employing MD simulations, the nanoscale contact behavior of substrates containing (1 1 1) planes parallel to their interface is studied. The study is conducted on three fcc metals (i.e., Al, Cu, and Ag) to investigate the effect of materials properties on contact behavior. Contact behavior is divided into two parts: (1) the JC behavior, and (2) the evolution of dislocation distribution and density after contact. In part (1), it is shown that JC occurs in all three metals, but Cu presents a smooth JC behavior, in contrast to Al and Ag, probably because of its higher Young's modulus and (1 1 1) surface energy. The major findings in part (2) are the following:

1- The dislocations that are present at the interface, due to the misorientation between substrates, may multiply, depending on other parameters. Dislocation multiplication significantly affects the distribution and density of dislocations in the system.
2- The chance of dislocation multiplication is higher at high contact temperatures, high strain values, and low misorientation angles close to 0°.
3- Dislocation multiplication is less likely to occur in Al than Cu or Ag.
4- The predominant mechanism by which dislocation multiplication occurs in Al is cross-slip of interfacial dislocations, but in Cu and Ag it is the nucleation of partial dislocations from the interface.

CRediT authorship contribution statement

Milad Khajehvand: Methodology, Software, Formal analysis, Investigation, Writing - original draft, Visualization, Data curation. **Henri Seppänen:** Writing - review & editing, Supervision, Funding acquisition. **Panthea Sepehrband:** Conceptualization, Validation, Resources, Writing - review & editing, Supervision, Project administration, Funding acquisition.

Acknowledgements

This work was supported by the National Science Foundation (CMMI-1728652), and the School of Engineering at Santa Clara University (FY1718IG).

Data availability

Data will be made available on request.

Appendix A. Supplementary data

Supplementary data to this article can be found online at https://doi.org/10.1016/j.commatsci.2019.109149.

References

[1] J.K. Gimzewski, R. Möller, Transition from the tunneling regime to point contact studied using scanning tunneling microscopy, Phys. Rev. B. 36 (1987) 1284–1287, https://doi.org/10.1103/PhysRevB.36.1284.
[2] C. Untiedt, M.J. Caturla, M.R. Calvo, J.J. Palacios, R.C. Segers, J.M. van Ruitenbeek, Formation of a metallic contact: jump to contact revisited, Phys. Rev. Lett. 98 (2007) 206801, , https://doi.org/10.1103/PhysRevLett. 98.206801.
[3] N. Agraït, J.G. Rodrigo, S. Vieira, Conductance steps and quantization in atomic-size contacts, Phys. Rev. B. 47 (1993) 12345–12348, https://doi.org/10.1103/PhysRevB.47.12345.
[4] J.M. Krans, C.J. Muller, I.K. Yanson, T.C.M. Govaert, R. Hesper, J.M. van Ruitenbeek, One-atom point contacts, Phys. Rev. B. 48 (1993) 14721–14724, https://doi.org/10.1103/PhysRevB.48.14721.
[5] J. Voets, R.J.P. Keijsers, O.I. Shklyarevskii, H. van Kempen, Effects of electrode interactions observed in a mechanically controllable break junction, Phys. Rev. B. 53 (1996) 1072–1075, https://doi.org/10.1103/PhysRevB.53.1072.
[6] U. Landman, W.D. Luedtke, N.A. Burnham, R.J. Colton, Atomistic mechanisms and dynamics of adhesion, nanoindentation, and fracture, Science 248 (1990) 454–461, https://doi.org/10.1126/science.248.4954.454.
[7] A. Fortini, M.I. Mendelev, S. Buldyrev, D. Srolovitz, Asperity contacts at the nanoscale: comparison of Ru and Au, J. Appl. Phys. 104 (2008) 074320, , https://doi.org/10.1063/1.2991301.
[8] J.B. Pethica, A.P. Sutton, On the stability of a tip and flat at very small separations, J. Vac. Sci. Technol. A Vacuum, Surfaces, Film. 6 (1988) 2490–2494, https://doi.org/10.1116/1.575577.
[9] J.R. Smith, G. Bozzolo, A. Banerjea, J. Ferrante, Avalanche in adhesion, Phys. Rev. Lett. 63 (1989) 1269–1272, https://doi.org/10.1103/PhysRevLett. 63.1269.
[10] P.-R. Cha, D.J. Srolovitz, T. Kyle Vanderlick, Molecular dynamics simulation of single asperity contact, Acta Mater. 52 (2004) 3983–3996, https://doi.org/10.1016/J.ACTAMAT.2004.05.014.
[11] M. Khajehvand, P. Sepehrband, The effect of crystallographic misorientation and interfacial separation on jump-to-contact behavior and defect generation in aluminum, Model. Simul. Mater. Sci. Eng. 26 (2018) 055007, , https://doi.org/10.1088/1361-651X/aac427.
[12] J. Huang, M. Meyer, V. Pontikis, Is pipe diffusion in metals vacancy controlled? A molecular dynamics study of an edge dislocation in copper, Phys. Rev. Lett. 63 (1989) 628–631, https://doi.org/10.1103/PhysRevLett. 63.628.
[13] M. Gholamirad, S. Soltani, P. Sepehrband, Dislocation assisted diffusion: a mechanism for growth of intermetallic compounds in copper ball bonds, Microelectron. Reliab. 81 (2018) 210–217, https://doi.org/10.1016/J.MICROREL.2017.12.038.
[14] H. Jiang, I. Szlufarska, Small-angle twist grain boundaries as sinks for point defects, Sci. Rep. 8 (2018) 3736, https://doi.org/10.1038/s41598-018-21433-7.
[15] S. Shao, J. Wang, A. Misra, R.G. Hoagland, Spiral patterns of dislocations at nodes in (111) semi-coherent FCC interfaces, Sci. Rep. 3 (2013) 2448, https://doi.org/10.1038/srep02448.
[16] H. Van Swygenhoven, P.M. Derlet, A. Hasnaoui, Atomic mechanism for dislocation emission from nanosized grain boundaries, Phys. Rev. B. 66 (2002) 024101, , https://doi.org/10.1103/PhysRevB.66.024101.
[17] D.E. Spearot, K.I. Jacob, D.L. McDowell, Dislocation nucleation from bicrystal interfaces with dissociated structure, Int. J. Plast. 23 (2007) 143–160, https://doi.org/10.1016/J.IJPLAS.2006.03.008.
[18] I.J. Beyerlein, J. Wang, R. Zhang, Mapping dislocation nucleation behavior from bimetal interfaces, Acta Mater. 61 (2013) 7488–7499, https://doi.org/10.1016/J.ACTAMAT.2013.08.061.
[19] S. Dai, Y. Xiang, D.J. Srolovitz, Atomistic, generalized Peierls-Nabarro and analytical models for (1 1 1) twist boundaries in Al Cu and Ni for all twist angles, Acta Mater. 69 (2014) 162–174, https://doi.org/10.1016/J.ACTAMAT.2014.01.022.
[20] J.T.M. De Hosson, V. Vitek, Atomic structure of (111) twist grain boundaries in f.c.c metals, Philos. Mag. A. 61 (1990) 305–327, https://doi.org/10.1080/01418619008234943.
[21] S. Dai, Y. Xiang, D.J. Srolovitz, Structure and energy of (1 1 1) low-angle twist boundaries in Al, Cu and Ni, Acta Mater. 61 (2013) 1327–1337, https://doi.org/10.1016/J.ACTAMAT.2012.11.010.
[22] S. Plimpton, Fast parallel algorithms for short-range molecular dynamics, J. Comput. Phys. 117 (1995) 1–19, https://doi.org/10.1006/JCPH.1995.1039.
[23] H.W. Sheng, M.J. Kramer, A. Cadien, T. Fujita, M.W. Chen, Highly optimized embedded-atom-method potentials for fourteen fcc metals, Phys. Rev. B. 83 (2011) 134118, , https://doi.org/10.1103/PhysRevB.83.134118.
[24] S. Nosé, A molecular dynamics method for simulations in the canonical ensemble, Mol. Phys. 52 (1984) 255–268, https://doi.org/10.1080/00268978400101201.
[25] W.G. Hoover, Canonical dynamics: equilibrium phase-space distributions, Phys. Rev. A. 31 (1985) 1695–1697, https://doi.org/10.1103/PhysRevA.31.1695.
[26] W.G. Hoover, Constant-pressure equations of motion, Phys. Rev. A. 34 (1986) 2499–2500, https://doi.org/10.1103/PhysRevA.34.2499.
[27] N. Agraït, A.L. Yeyati, J.M. van Ruitenbeek, Quantum properties of atomic-sized conductors, Phys. Rep. 377 (2003) 81–279, https://doi.org/10.1016/S0370-1573(02)00633-6.
[28] A. Stukowski, V.V. Bulatov, A. Arsenlis, Automated identification and indexing of dislocations in crystal interfaces, Model. Simul. Mater. Sci. Eng. 20 (2012) 085007, , https://doi.org/10.1088/0965-0393/20/8/085007.
[29] A. Stukowski, Visualization and analysis of atomistic simulation data with OVITO–the open visualization tool, Model. Simul. Mater. Sci. Eng. 18 (2010) 015012, , https://doi.org/10.1088/0965-0393/18/1/015012.
[30] J. Friedel, Regarding Seeger's Paper on Work Hardening, in: J.C. Fisher, W.G. Johnston, R. Thomson, T. Vreeland (Eds.), Dislocations Mech. Prop. Cryst. John Wiley & Sons Inc, 1957, pp. 330–332.
[31] B. Escaig, Sur le glissement dévié des dislocations dans la structure cubique à faces centrées, J. Phys. 29 (1968) 225–239, https://doi.org/10.1051/jphys:01968002902-3022500.
[32] W. Püschl, Models for dislocation cross-slip in close-packed crystal structures: a critical review, Prog. Mater. Sci. 47 (2002) 415–461, https://doi.org/10.1016/S0079-6425(01)00003-2.
[33] J.P. Hirth, J. Lothe, Theory of dislocations, 2nd ed., Wiley, 1982.
[34] H. Van Swygenhoven, P.M. Derlet, A.G. Frøseth, Stacking fault energies and slip in nanocrystalline metals, Nat. Mater. 3 (2004) 399–403, https://doi.org/10.1038/nmat1136.
[35] M. Jo, Y.M. Koo, B.-J. Lee, B. Johansson, L. Vitos, S.K. Kwon, Theory for plasticity of

face-centered cubic metals, Proc. Natl. Acad. Sci. 111 (2014) 6560–6565, https://doi.org/10.1073/PNAS.1400786111.
[36] J.R. Rice, Dislocation nucleation from a crack tip: an analysis based on the Peierls concept, J. Mech. Phys. Solids. 40 (1992) 239–271, https://doi.org/10.1016/S0022-5096(05)80012-2.
[37] D. Rodney, J. Bonneville, Dislocations, Phys. Metall. Elsevier, 2014, pp. 1591–1680, , https://doi.org/10.1016/B978-0-444-53770-6.00016-2.
[38] Y. Kamimura, K. Edagawa, S. Takeuchi, Experimental evaluation of the Peierls stresses in a variety of crystals and their relation to the crystal structure, Acta Mater. 61 (2013) 294–309, https://doi.org/10.1016/J.ACTAMAT.2012.09.059.
[39] D. Hull, D.J. Bacon, Introduction to Dislocations, 5th ed., Butterworth-Heinemann, 2011.
[40] E. Oren, E. Yahel, G. Makov, Kinetics of dislocation cross-slip: a molecular dynamics study, Comput. Mater. Sci. 138 (2017) 246–254, https://doi.org/10.1016/J.COMMATSCI.2017.06.039.